Nanoscale

Accepted Manuscript

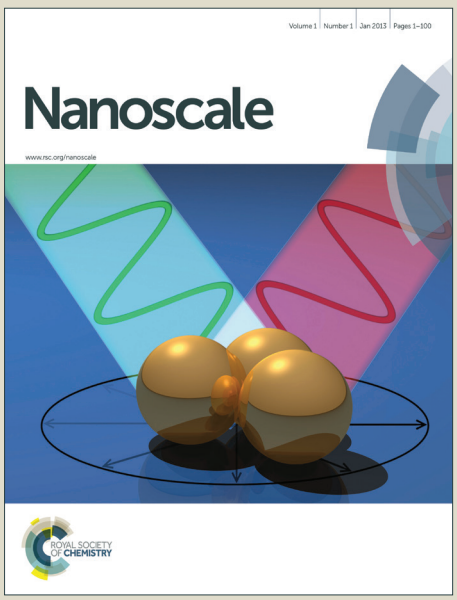

ROYAL SOCIETY OF CHEMISTRY

www.rsc.org/nanoscale

Journal Name

RSCPublishing

ARTICLE

Geometric Nonlinearity and Mechanical Anisotropy in Strained Helical Nanoribbons

Cite this: DOI: 10.1039/xoxxoooooox

Z. Chen[a]

Received ooth January 2012,
Accepted ooth January 2012

DOI: 10.1039/xoxxoooooox

www.rsc.org/

Fabrication and synthesis of helical nanoribbons have received increasing attention because of the broad applications of helical nanostructures in nano-elecromechanical/ micro-electromechanical systems (NEMS/MEMS), sensors, active materials, drug delivery, etc. Here I study the mechanical principles in designing strained helical nanoribbons, and propose the use of a full three-dimensional finite element method to simulate the coexistence of both left- and right-handed segments in the same strained nanoribbon. This work can both help understand the large deformation behaviours of such nanostructures and assist the design of helical nanostructures for engineering applications.

1 Introduction

Helical structures are among the most universal shapes in nature and engineering materials [1]. Helical shapes arise in many natural systems, including DNA [2], chiral seed pods [3], tendrils of plants [4-6], etc. Mechanical self-assembly of helical structures has received continuous attention from the research community because of the potential applications in nano-elecromechanical/ micro-electromechanical systems (NEMS/MEMS), sensors [7], microrobotics [8], active materials [9], drug delivery [10], and optoelectronics [11].

Helical ribbon shapes often result from the competition between bending and stretching energy, as well as the work done by a variety of driving forces [3, 12-22], including but not limited to, surface stresses [12-15], residual stresses [5, 16], misfit strains [18-21], piezoelectricity [22], differential growth [23, 24], and swelling/de-swelling [3, 25]. The transition between different helical shapes, for instance, the purely twisted and nearly cylindrical helical shapes, can occur due to the complex interplay between the molecular interactions, chiral twists, and ribbon elasticity [26-30]. While the selection of shapes typically relies on the detailed mechanisms involved in an individual system [26-33], some universal features exist regardless of the kinematics involved in such change in geometry stay the same [10, 11].

In strained helical nanoribbons, the main driving force is the misfit strain between different layers. A remarkable feature in such "nanomechanical architectures" is the versatile combination of materials that can be used [34-39]. Although the analytic solution exists for predicting the rolling radius in such strained nanostructures, more complex behaviours, such as the co-existence of both left- and right-handed components [18], the change of chirality [5, 16, 18, 19, 37], and multistability [40-49], still remain to be explored.

Noticeably, Zhang et al. [19] reported the anomalous coiling behaviours in SiGe/Si and SiGe/Si/Cr nanohelices. Specifically, as the width decreases from 1.3μm to to 0.7 μm, the pitch and helix angle of the SiGe/Si/Cr helical nanobelt first decrease, then increase, and finally decrease until a self-overlapping multi-turn ring forms when the width is reduced to 0.7 μm. During this process, the chirality also changes from right-handed to mixed and to left-handed, in addition to the variance of pitch, helix angle and geometric orientation. To interpret this novel phenomenon, Zhang et al. considered the edge effects and hypothesized that the edge stress will become increasingly dominating, resulting in the change of chirality, and the eventual self-overlapping ring shape when the ribbon width falls below a threshold [19]. Dai and Shen further employed a Cosserat rod theory to explain the mechanical mechanism by again considering the rising edge effects as the width decreases [36]. Not only can the chirality of strained seminconductor nanohelices change under certain circumstances, but there can also exist helical nanoribbons with co-exisiting left-handed and right-handed segments. These helical nano-structures have important applications in micro-capacitors, inductors [18], and

motion converters [37]. Interestingly, when there is self-contact, a shape transition into a tightly-coiled helical structure with only one handedness can occur [50].

In this work, I study the mechanical principles involved in designing strained helical nanoribbons, in particular, principles related to engineering the pitch, radius, orientation and chirality of helical nanoribbons. Furthermore, a finite element method is used to simulate the spontaneous deformation of strained nanoribbons with both left-handed and right-handed segments. This work can promote understanding of the mechanical self-assembly principle of three-dimensional chiral structures, and aid the programmable design and manufacturing of spontaneously helical nanostructures for NEMS and MEMS applications.

2 Results and discussion

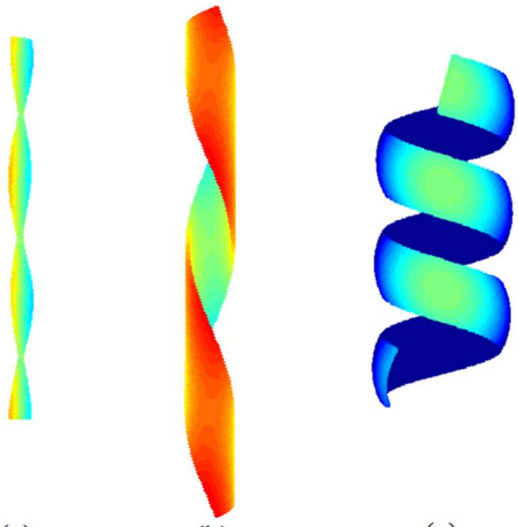

Fig.1 Helical ribbon shapes with different Gaussian curvature . $\kappa_G = \kappa_1\kappa_2$. , where κ_1 and κ_2 are the principal curvatures. (a) $\kappa_G < 0$; (b) $\kappa_G = 0$; (c) $\kappa_G > 0$.

Helical ribbon shapes often result from anisotropic mechanical stresses and geometric mis-alignment between the principal axes of the driving force and the geometric axes of the ribbon (i.e., the length and width directions) [12, 13]. Previous studies [12, 13] have shown that four independent parameters, κ_1, κ_2, $\emptyset$ and w control the shape of a helical ribbon (where $\emptyset$ is the misorientation angle, and w is the width of the ribbon). A purely twisted ribbon (Fig. 1a) forms when $\kappa_1 cos^2\emptyset + \kappa_2 sin^2\emptyset = 0$ (with a negative Gaussian curvature, i.e., $\kappa_G < 0$); when either κ_1 or κ_2 vanishes ($\kappa_G = 0$), the ribbon forms a cylindrical helical ribbon; when $\kappa_G > 0$, a general helical ribbon with concave edge results (Fig.1c). Moreover, recent studies have shown that geometric nonlinearity can give rise to selection of shape and multi-stability in helical ribbons [33].

To study the anomalous coiling of nanoribbons, I noticed that in Zhang et al's study [19] the width around which the SiGe/Si/Cr nanobelt switches shape from a helical ribbon to a ring shape is 0.8 μm or 0.7 μm. The corresponding value of the dimensionless parameter, $\eta = w\sqrt{\kappa/h}$ [3, 15], is around 3.27 or 2.85, in the same order of magnitude as the critical value $\eta_c = \sqrt[4]{80(1+\nu)/3} \approx 2.4$. Therefore, it is worth investigating whether geometric nonlinearity plays a role in the anomalous coiling of these strained helical ribbons. Taking into account the nonlinear geometric effects (competition between bending and stretching), the ribbon, when subjected to an equal biaxial misfit strain, adopts a ring shape [12, 13]. This result is consistent with the experimental observation in SiGe/Si/Cr nanobelts. I then calculated the value of η at which the change of chirality occurs (w = 1.1 μm) to 4.5 >> η_c, so the ribbon is still in the regime ($\eta >> \eta_c$) where it should form a nearly cylindrical helical shape because of geometric nonlinearity. Moreover, due to nonlinear geometric effects [3, 15], bistable behaviors can occur resulting in the change of helical pitch, radius and orientation [33]. While there are similar characteristics between the shape transition of bistable helical ribbons and the anomalous coiling of strained helical nanoribbons, there is no change in chirality in the previous phenomena. Therefore, I suggest that geometric nonlinearity may not be the main reason for the anomalous coiling, and that instead, the increasingly significant edge stresses (when the width decreases) are the main cause for such behaviors, as previously hypothesized by the researchers. In fact, this principle can be employed to design and manufacture nanostructures with applications in MEMS/NEMS.

Nevertheless, the geometric nonlinearity can still play an important role in generating cylindrical helical ribbons in a lot of cases, and can possibly be exploited in designing multistable strained semiconductor structures. The interaction between the geometric nonlinear effects and mechanical anisotropy in crystalline materials remains to be explored.

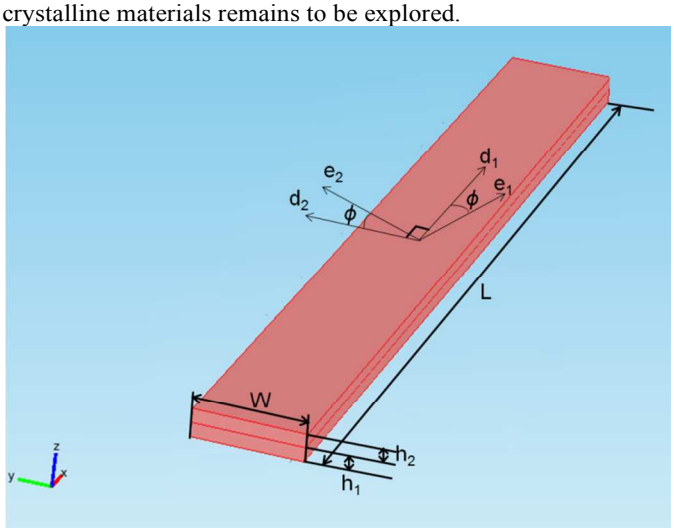

Fig. 2 Geometry of a bilayer strained nanoribbon before releasing from the substrate.

Here, it is worth noting that the existence of mechanical anisotropy due to preferred rolling along the most compliant direction adds another dimension to the tunability of designing helical nanostructures. Along with this type of mechanical anisotropy comes the difficulty in modeling spontaneous

deformation due to lattice mismatch. In this work, this difficulty is overcome by assuming the material properties to be isotropic and linear elastic, while suppressing the misfit strain along the direction perpendicular to the most compliant bending direction. By so doing, similar deformation can be achieved as compared to the mechanically anisotropic system of interest.

For a bilayer strained heterostructure [38] (Fig. 2), the radius is given analytically by $R = (h_1^4 + 4\alpha h_1^3 h_2 + 6\alpha h_1^2 h_2^2 + 4\alpha h_1 h_2^3 + \alpha^2 h_2^4)/[6\varepsilon_0\alpha(1+v)h_1 h_2 (h_1 + h_2)]$. Here, I point out that since R~h/ε_0, it is convenient to simulate this large deformation using the set of parameters $(a\varepsilon_0, ah_1, ah_2)$ instead of $(\varepsilon_0, h_1, h_2)$ for an arbitrary possible value of a. This can be useful when the numerical issue emerges as the thickness becomes too small (at the nanoscale).

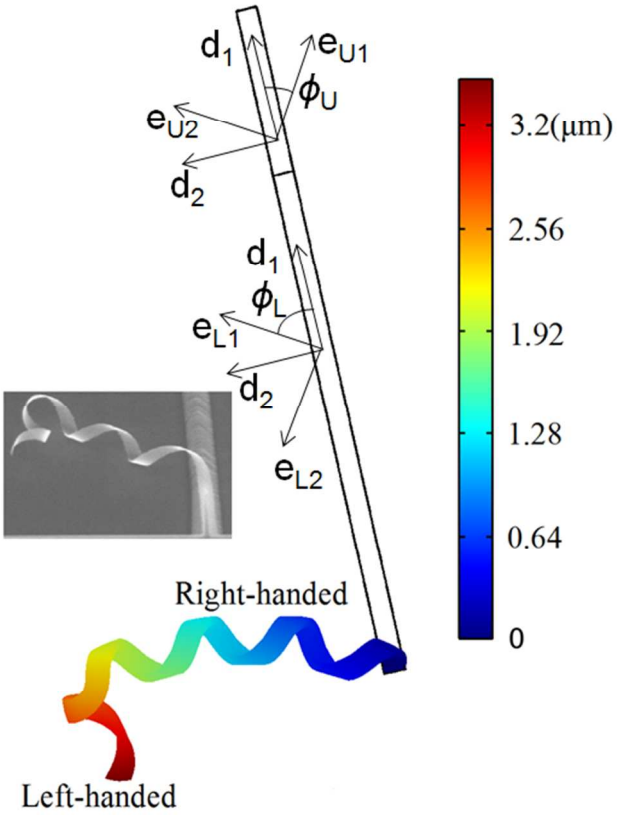

Fig. 3. A helical nanoribbon with both left-handed and right-handed segments with only one fixed end. Here, $\emptyset_L = 50°$, $\emptyset_U = 40°$ and $\varepsilon_0 = 0.05$. In the upper segment (of length 0.8 μm), the effective misfit strain tensor of the bottom layer is $\varepsilon_b = \varepsilon_0 e_{U2} \otimes e_{U2}$. In the lower segment (of length 2.4 μm), the effective misfit strain tensor of the bottom layer is $\varepsilon_b = \varepsilon_0 e_{L2} \otimes e_{L2}$. Inset: (adapted from Fig. 7 by Zhang et al. [18]). The color indicates the total displacement.

While the analytical solution exists for the simplest case where the strained nanoribbon adopts a cylindrical (helical) shape and the Poisson's ratio is constant throughout multiple layers, there are scenarios where such solution may not exist. For example, there could be co-existing left-handed and right-handed segments in SiGe/Si/Cr nanobelts where the mis-alignment angle is slightly larger than 45 degrees and the tip has an influence in the preferred chirality [18, 37]. While qualitative interpretation of such behaviour was provided, quantitative modelling remains a challenge. To this end, I employ a finite element method [20, 49] to simulate this process (Fig. 3). A strained nanoribbon of length L = 3.2 μm, width w = 0.1 μm, thickness $h_1 = h_2 = 5nm$, and misfit strain $\varepsilon_0 = 0.05$ is divided into two connecting segments of length 0.8 μm and 2.4 μm, respectively. The misalignment angle (between the ribbon's long axis and the preferred bending axis <100>) in the lower segment ribbon is 50 degrees, and the mis-alignment angle in the upper segment is also 50 degrees. The deformed shape exhibits co-existence of both left- and right-handed parts connected by a perversion [5, 16, 18], consistent with the experimental result by Zhang et al. [18] (inset of Fig. 3). Here, it is worth mentioning that it is important to incorporate geometric nonlinearity in the finite element simulations.

Next, I use this framework to study the spontaneous deformation of a V-shaped mesa design. Fig. 4 shows the geometric parameter involved in such a mesa shape. It can be shown that the angles satisfy the geometric relationship: $2\alpha + \emptyset_1 + \emptyset_2 = 270°$. In order to develop symmetric left- and right-handed helical shapes, $\emptyset_1$ should be equal to $\emptyset_2$. An example is given in Fig. 5, where $\emptyset_1 = \emptyset_2 = 75°$, and $\alpha = 60°$.

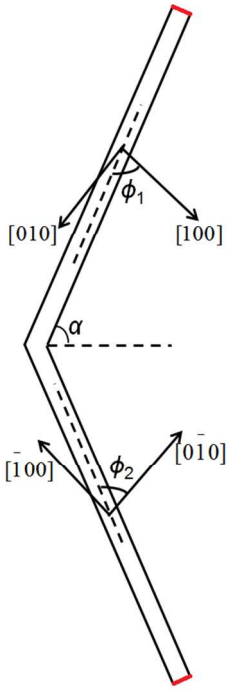

Fig. 4 Geometry of a symmetric mesa design. Both ends (in red) are fixed.

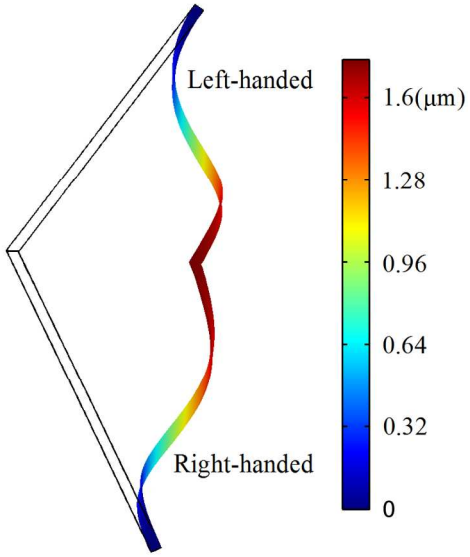

Fig. 5 A strained nanoribbon with symmetric left-handed and right-handed segments (both ends being fixed). Here, $\emptyset_1 = \emptyset_2 = 75°$, $\varepsilon_0 = 0.024$. In the upper segment, the effective misfit strain tensor of the bottom layer is $\varepsilon_b = \varepsilon_0 e_{U1} \otimes e_{U1}$, where e_{U1}=[100] and e_{U2}=[010]. In the lower segment, the effective misfit strain tensor of the bottom layer is $\varepsilon_b = \varepsilon_0 e_{L1} \otimes e_{L1}$, where $e_{L1} = [0\bar{1}0]$ and $e_{L2} = [\bar{1}00]$. The color indicates the total displacement.

Yet another example of the application of the current methodology is the design of asymmetric helical shapes with both left- and right-handed components. This can be achieved by having $\emptyset_1 \neq \emptyset_2$. In Fig. 6, for instance, $\emptyset_1 = 86°, \emptyset_2 = 64°$, when $\alpha = 60°$ The resulting shape is similar in nature to the helical nanostructure developed by Zhang et al. [18].

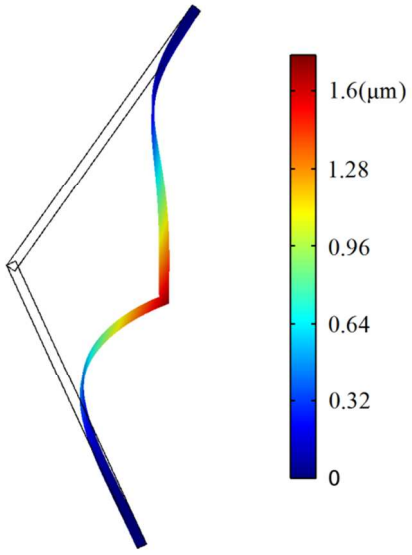

Fig. 6 A strained nanoribbon with asymmetric left-handed and right-handed segments (both ends being fixed). Here, $\emptyset_1 = 86°, \emptyset_2 = 64°$ $\varepsilon_0 = 0.01$. Here, $\emptyset_1 = \emptyset_2 = 75°$ and $\varepsilon_0 = 0.024$. In the upper segment, the effective misfit strain tensor of the bottom layer is $\varepsilon_b = \varepsilon_0 e_{U1} \otimes e_{U1}$, where e_{U1}=[100] and e_{U2}=[010]. In the lower segment, the effective misfit strain tensor of the bottom layer is $\varepsilon_b = \varepsilon_0 e_{L1} \otimes e_{L1}$, where $e_{L1} = [0\bar{1}0]$ and $e_{L2} = [\bar{1}00]$. The color indicates the total displacement.

Finite Element Simulations

The finite element model used in this work is a full three-dimensional model using the structural mechanics module of Comsol Multiphysics V4.3a with the methodology detailed in the references [20, 49]. I employed this model here to study that the shape transition and multi-stability in helical ribbon structures driven by misfit or residual strains between different layers in an initially flat elastic ribbon [3, 12, 13, 19]. The Young's modulus of Si is 168.9GPa, and that of SiGe is 161.2GPa [35]. The Poisson's ratio of both layers are 0.27 [36].

Conclusions

In this work, I explored the mechanical principles involved in designing helical nanoribbons through strain engineering. I discussed the possibility of exploiting geometric nonlinearity and mechanical anisotropy to shape strained helical nanoribbons. Furthermore, I employed three-dimensional finite element simulations to study the more complicated cases where both left-handed and right-handed components exist in one ribbon, with either one end or both ends fixed. The results of this study can complement the recent theoretical, experimental and computational studies on the mechanical self-assembly of spontaneous helical structures and multi-stable structures, and will promote quantitative understanding of engineering shapes in these nanostructures. This work can also facilitate the programmable design of functional nanostructures with a variety of potential applications in NEMS/MEMS, sensors, drug delivery, active materials, optoelectronics, and bio-inspired robotics.

Acknowledgements

Z. C. is supported by Society in Science, The Branco Weiss Fellowship, administered by ETH Zurich.

Notes and references

[a] Department of Biomedical Engineering, Washington University, St. Louis 63130, USA.

[1] N. Chouaieb, A. Goriely and J.H. Maddocks, Proc. Natl. Acad. Sci. USA, 2006, 103, 9398-9430.

[2] Y.Y. Biton, B.D. Coleman, and D. Swigon, J. Elast., 2007, 87, 187-210.

[3] S. Armon, E. Efrati, R. Kupferman and E. Sharon, Science, 2011, 333, 1726-1730.
[4] A. Goriely and M. Tabor, Phys. Rev. Lett., 1998, 80, 1564-1568.
[5] S.J. Gerbode, J.R. Puzey, A.G. McCormick and L. Mahadevan, Science, 2012, 337, 1087–1091.
[6] J. Wang, G. Wang, X. Feng, T. Kitamura, Y. Kang, S. Yu and Q. Qin, Sci. Rep., 2013, 3, 3102.
[7] Y. Sawa, K. Urayama, T. Takigawa, V. Gimnez-Pinto, B.L. Mbanga, F, Ye, J.V. Selinger and R.L.B. Selinger, Phy. Rev. E, 2013, 88, 022502.
[8] J.J. Abbott, K.E. Peyer, M.C. Lagomarsino, L. Zhang, L.X. Dong, I.K. Kaliakatsos and B.J. Nelson, Int. J. Robot. Res., 2009, 28, 1434-1447.
[9] Q. Ge, H.J. Qi and M.L. Dunn, Appl. Phys. Lett., 2013, 103, 131901.
[10]I.W. Hamley, A. Dehsorkhi, V. Castelletto, S. Furzeland, D. Atkins, J. Seitsonen, J. Ruokolainen, Soft Matter, 2013, 9, 9290-93.
[11]G. Hwang, C. Dockendorf, D. Bell, L. Dong, H. Hashimoto, D. Poulikakos and B. Nelson, Int. J. Optomechatronics, 2008, 2, 88-103.
[12]Z. Chen, C. Majidi, D.J. Srolovitz and M. Haataja, Appl. Phys. Lett., 2011, 98, 011906.
[13]Z. Chen, C. Majidi, D.J. Srolovitz and M. Haataja, 2012, arXiv:1209.3321.
[14]J. Wang, X. Feng, G. Wang and S. Yu, Appl. Phys. Lett., 2008, 92, 191901.
[15]Z. Chen, Q. Guo, C. Majidi, W. Chen, D.J. Srolovitz and M.Haataja, Phys. Rev. Lett., 2012, 109, 114302.
[16]J. Huang, J. Liu, B. Kroll, K. Bertoldi and D.R. Clarke, Soft Matter, 2012, 8, 6291-6300.
[17]Q. Guo, Z. Chen, W. Li, P. Dai, K. Ren, J. Lin, L.A. Taber and W. Chen, arXiv:1312.0663.
[18]L. Zhang, E. Deckhardt, A. Weber, C. Schonenberger and D. Grutzmacher, Nanotechnology, 2005, 16, 655.
[19]L. Zhang, E. Ruh, D. Grützmacher, L. Dong, D.J. Bell, B.J. Nelson, and C. Schönenberger, Nano Lett., 2006, 6, 1311-1317.
[20]Q. Guo, H. Zheng, W. Chen and Z. Chen, J. Mech. Med. Biol., 2013, 13, 1340018.
[21]Z. Suo, E.Y. Ma, H. Gleskova and S. Wagner, Appl. Phys. Lett., 1999, 74, 1177.
[22]C. Majidi, Z. Chen, D.J. Srolovitz and M. Haataja, J. Mech. Phys. Solids, 2010, 58, 73–85.
[23]T. Savin, N.A. Kurpio, A.E. Shyer, P. Florescu, H. Liang, L. Mahadevan and C.J. Tabin, Nature, 2011, 476, 57-62.
[24]M.A. Wyczalkowski, Z. Chen, B.A. Filas, V.D. Varner and L.A. Taber, Birth Defects Research Part C: Embryo Today, 2012, 96, 132-152.
[25]W. Li, G. Huang, H. Yan, J. Wang, Y. Yu, X. Hu, X. Wu and Y. Mei, Soft Matter, 2012, 7103-7107.
[26]Y. Sawa, F. Ye, K. Urayama, T. Takigawa, V. Gimenez-Pinto, R.L.B. Selinger and J.V. Selinger, Proc Nat Acad Sci USA, 2011, 108, 6364-6368.
[27]J.V. Selinger, M.S. Spector and J.M Schnur, J. Phys. Chem. B, 2001, 105, 7157-7169.
[28]R. Oda, I. Huc, M. Schmutz, S.J. Candau and F.C. MacKintosh, Nature, 1999, 399, 566-569.
[29]L. Teresi and V. Varano, Soft Matter, 2012, 9, 3081-3088.
[30]T. Gibaud, E. Barry, M.J. Zakhary, M. Henglin, A. Ward, Y. Yang, C. Berciu, R. Oldenbourg, M.F. Hagan, D. Nicastro, R.B. Meyer and Z. Dogic, Nature, 2012, 481, 348-351.
[31]W.S. Childers, N.R. Anthony, A.K. Mehta, K.M. Berland and D.G. Lynn, Langmuir, 2012, 28, 6386–6395.
[32]G. Bellesia, M.V. Fedorov and E.G. Timoshenko, J. Chem. Phys., 2008, 128, 195105.
[33]Q. Guo, A.K. Mehta, M.A. Grover, W. Chen, D.G. Lynn and Z. Chen, Appl. Phys. Lett., arXiv:1312.3571., in press.
[34]M. Huang, C. Boone, M. Roberts, D.E. Savage, M.G. Lagally, N. Shaji, H. Qin. R. Blick, J.A. Nairn and F.Liu, Adv. Mater., 2005, 17, 2860-2864.
[35]M. Huang, F. Cavallo, F. Liu, and M.G. Lagally, Nanoscale, 2011, 3, 96.
[35]L. Dai and L. Zhang, Nanoscale, 2013, 5, 971.
[36]L. Dai and W.Z. Shen, J. Appl. Phys., 2009, 106, 114314.
[37]L. Dong, L. Zhang, B.E. Kratochvil, K. Shou and B.J. Nelson, J. Micro. Sys., 2009, 18, 1047.
[38]M. Grundmann, Appl. Phys. Lett., 2003, 83, 2444.
[39] P. Froeter, X. Yu, W. Huang, F. Du, M. Li, I. Chun, S.H. Kim, K.J. Hsia, J.A. Rogers and X. Li, Nanotechnology, 2013, 24, 475301.
[40]R. Ghafouri and R. Bruinsma, Phys. Rev. Lett., 2005, 94, 138101.
[41]E. Kebadze, S.D. Guest and S. Pellegrino, Int. J. Solids Struct., 2004, 41, 2801-2820.
[42]S. Daynes, C.G. Diaconu, K.D. Potter, P.M. Weaver, J. Compos. Mater., 2010, 44, 1119-1137.
[43]S. Vidoli and C. Maurini, Proc. R. Soc. A, 2008, 464, 2949-2966.
[44]X. Lachenal, P.M. Weaver and S. Daynes, Proc. R. Soc. A, 2012, 468, 1230-51.
[45]Y. Forterre, J.M. Skothelm, J. Dumais and L. Mahadevan, Nature, 2005, 433, 421-425.
[46]H. Zheng, Y. Liu and Z. Chen, J. Postdoctoral Research, 2013, 1, 40-50.
[47]M. Shahinpoor, Bioinsp. Biomim., 2011, 6, 046004.
[48]A.F. Arrieta, P. Hagedorn, A. Erturk and D.J. Inman, Appl. Phys. Lett., 2010, 97, 104102.
[49]Q. Guo, H. Zheng, W. Chen and Z. Chen, Z, Bio-Med. Mater. Eng., 2014, 24, 557–562.
[50] Q. Guo, Z. Chen, W. Li, P. Dai, K. Ren, J. Lin, L.A. Taber, and W. Chen., EPL, 2014, 105, 64005.